IOPscience iopscience.iop.org

Home Search Collections Journals About Contact us My IOPscience

Ground-state and spin-wave dynamics in Brownmillerite $SrCoO_{2.5}$—a combined hybrid functional and LSDA + *U* study

This content has been downloaded from IOPscience. Please scroll down to see the full text.

2014 J. Phys.: Condens. Matter 26 036004

(http://iopscience.iop.org/0953-8984/26/3/036004)

View the table of contents for this issue, or go to the journal homepage for more

Download details:

IP Address: 128.219.49.14
This content was downloaded on 20/12/2013 at 21:24

Please note that terms and conditions apply.

IOP Publishing Journal of Physics: Condensed Matter
J. Phys.: Condens. Matter **26** (2014) 036004 (7pp) doi:10.1088/0953-8984/26/3/036004

Ground-state and spin-wave dynamics in Brownmillerite $SrCoO_{2.5}$—a combined hybrid functional and LSDA + *U* study

Chandrima Mitra, Randy S Fishman, Satoshi Okamoto, Ho Nyung Lee and Fernando A Reboredo

Materials Science and Technology Division, Oak Ridge National Laboratory, Oak Ridge, TN 37831, USA

E-mail: mhc@ornl.gov

Received 17 September 2013
Accepted for publication 22 November 2013
Published 20 December 2013

Abstract

We theoretically investigate the ground-state magnetic properties of the brownmillerite phase of $SrCoO_{2.5}$. Strong correlations between Co d electrons are treated within the local spin density approximations of density functional theory (DFT) with Hubbard U corrections (LSDA + U), and results are compared with those using the Heyd–Scuseria–Ernzerhof (HSE) functional. The parameters computed with a U value of 7.5 eV are found to match closely to those computed within the HSE functional. A G-type antiferromagnetic structure is found to be the most stable one, consistent with experimental observation. By mapping the total energies of different magnetic configurations onto a Heisenberg Hamiltonian, we compute the magnetic exchange interaction parameters, J, between the nearest-neighbor Co atoms. The J values obtained are then used to compute the spin-wave frequencies and inelastic neutron scattering intensities. Among four spin-wave branches, the lowest energy mode was found to have the largest scattering intensity at the magnetic zone center, while the other modes become dominant at different momenta. These predictions can be tested experimentally.

Keywords: magnetism, electronic structure, spin-wave

(Some figures may appear in colour only in the online journal)

1. Introduction

The diverse physical properties exhibited by perovskite oxides (ABO_3) make them an important class of materials. They range from ferroelectricity [1] and magnetism [2] to colossal magnetoresistance and superconductivity [3]. This interplay between structural, magnetic, and transport properties makes perovskites particularly interesting. Among the perovskites, cobalt-based materials are becoming increasingly popular as a replacement for platinum in catalytic converters in diesel vehicles [4]. Moreover, those with oxygen vacancies have been reported to show high oxygen mobility, which makes them promising candidates for use in catalysis, gas sensing, or as an oxygen membrane in solid-oxygen fuel cells [5]. These oxygen-deficient perovskites ($ABO_{3-\delta}$) show subtle changes in their physical properties compared to their bulk counterparts [6, 7]. $SrCoO_{3-\delta}$ is one such example. While stoichiometric $SrCoO_3$ has a cubic perovskite structure, its crystal structure is considerably modified depending on the amount of oxygen vacancies in it [8–10]. More specifically the oxygen-deficient $SrCoO_{3-\delta}$ shows a wide variety of phase changes when δ varies from 0.25 to 0.5 [8–10].

$SrCoO_{2.5}$ is particularly interesting because the oxygen vacancies form an ordered arrangement. The brownmillerite-type structure is formed by quenching this oxygen-deficient compound in liquid N_2 [11], which orders the oxygen vacancies. The crystal structure of $SrCoO_{2.5}$ is composed of alternating CoO_6 octahedron and CoO_4 tetrahedron layers along the x axis or the c axis, depending on the choice of convention [12, 13]. It can be derived from the perovskite structure by ordering oxygen vacancies along the [011] direction when the alternating octahedron and tetrahedron

 © 2014 IOP Publishing Ltd Printed in the UK

layers lie along the x-axis. Indeed, if additional oxygen atoms are forced into these deficient positions under high pressure, the perovskite structure is subsequently restored [8, 11]. In a recent experimental study by Choi *et al* [25], the reversal of the lattice and electronic structure evolution in $SrCoO_x$ ($x = 2.5$–3) was directly observed using real-time spectroscopic ellipsometry. They showed that the two phases ($SrCoO_{2.5}$ and $SrCoO_3$) 'could be reversibly controlled by changing the ambient pressure at greatly reduced temperatures'. While the stoichiometric perovskite, $SrCoO_3$, is a ferromagnet and a metal, experimental observations indicate that the brownmillerite phase, $SrCoO_{2.5}$, is antiferromagnetic and insulating, with a Néel temperature of about 570 K [14].

The goal of this paper is to study the electronic structure and ground-state magnetic properties of $SrCoO_{2.5}$. As is well known, within density functional theory (DFT), commonly used local and semi-local approximations to the exchange correlation functional, such as the local density approximation (LDA) and generalized gradient approximation (GGA), fail to produce an accurate description of the electronic structure. In particular, the computed band gaps of semiconductors and insulators are underestimated within these approximations. Hence one needs to go beyond LDA or GGA in order to improve on this shortcoming. In order to address this issue we will employ two different approaches to compute the electronic structure of $SrCoO_{2.5}$. As will be discussed in detail in section 2, the first is the so-called local spin density $+U$ (LSDA $+ U$) approximation, which applies a Hubbard U-like 'correction' to the strongly correlated orbitals, which in our case are the Co d orbitals. However, although computationally cheap, U remains an empirical parameter here. A different route is the application of hybrid functionals which corrects for self-interaction errors. A comparative study of these two functionals would then allow us to obtain an 'optimal' value of the U parameter in the LSDA $+ U$ calculations.

In order to compute the magnetic exchange interaction parameters between the Co atoms we rely on a mean-field Heisenberg Hamiltonian. A Heisenberg model with only nearest-neighbor interactions will be used to fit the interaction parameters J to the total energies obtained within DFT. Henceforth, Co atoms lying on the octahedral plane will be referred to as Co_{oct}, while those lying on the tetrahedral plane will be denoted as Co_{tet}. We find that all the interaction parameters J are negative. They include couplings within the octahedral and the tetrahedral plane as well as couplings between the two planes. The ground-state magnetic configuration is hence found to be a G-type configuration, in agreement with experimental findings [14]. From the computed values of the interaction parameters, we predict the spin dynamics of the system using a $1/S$ expansion starting from the classical ground state [15, 16].

The rest of the paper is organized in the following manner. Section 2 provides the computational details, section 3 presents the results for the magnetic interaction parameters, in section 4 the spin-wave formalism and results are discussed, and finally we draw our conclusions in section 5.

2. Computational method

The electronic structure calculations were performed within DFT employing the Vienna *ab initio* simulation package (VASP) code [17]. The projector augmented wave pseudopotentials (PAW) were used [18]. The valence electrons included for Sr, Co and O are $4s^2 4p^6 5s^2$, $3s^2\ 3p^6 4s^2 3d^2$, and $2s^2 2p^4$, respectively, and a plane-wave cut-off energy of 600 eV was used. A Monkhorst–Pack special k-point grid [19] of $4 \times 6 \times 6$ was chosen to integrate over the Brillouin zone. The energies converged to within 10^{-6} eV/cell. All forces converged within 0.004 eV/Å.

For the LSDA $+ U$ calculations, we used the simplified or the rotationally invariant approach as introduced by Dudarev *et al* [20]; this is implemented in the VASP code. Within this approach the LSDA $+ U$ functional is written as

$$E_{\mathrm{LSDA}+U} = E_{\mathrm{LSDA}} + \frac{U-J}{2}\sum_{\sigma}[\mathrm{Tr}\,\rho^{\sigma} - \mathrm{Tr}\,(\rho^{\sigma}\rho^{\sigma})], \quad (1)$$

where ρ^{σ} is the density matrix of d electrons. U and J are the spherically averaged matrix elements of the screened Coulomb electron–electron interaction. In order to determine an 'optimal' value of the U parameter, we compared the results to those of a hybrid functional calculation which is known to improve the band gaps for many semiconductors and insulators. We specifically used the Heyd–Scuseria–Ernzerhof (HSE) functional as implemented in VASP.

Within the HSE formalism [21], the exchange correlation functional is constructed from a fraction of the Hartree–Fock exchange (E_x) and the generalized gradient approximation due to Perdew, Burke, and Ernzerhof (PBE) [22]. The method has an advantage over the PBEh [23] hybrid functional due to its faster convergence. This is because, in the HSE method, as proposed by Heyd *et al* [24], the exact nonlocal exchange is further decomposed into a long-range part and a short-range part in real space. The range separation is determined by a parameter, μ, which is typically chosen as a distance at which the nonlocal long-range interaction becomes negligible. The HSE exchange correlation functional is written as

$$E_{\mathrm{xc}}^{\mathrm{HSE}} = \alpha E_x^{\mathrm{sr},\mu} + (1-\alpha)E_x^{\mathrm{PBE,sr},\mu} + E_x^{\mathrm{PBE,lr},\mu} + E_{\mathrm{c}}^{\mathrm{PBE}}, \quad (2)$$

where α is called the 'mixing parameter'; it accounts for the amount of Hartree–Fock-like exchange in the exchange correlation functional. The superscripts sr and lr denotes the short-range part and the long-range part, respectively, and μ refers to the screening parameter as mentioned earlier. The HSE calculation yields a band gap of 0.6 eV. We find that this corresponds to a U of 7.5 eV. We keep the J parameter fixed to 1 eV. From optical absorption spectra, Lee *et al* [25] obtained a band gap of 0.35 eV at 300 K, which opened up to 0.45 eV at 5 K.

3. Results and discussions

The orthorhombic unit cell of brownmillerite $SrCoO_{2.5}$ is shown in figure 1. Although the assignment of space group to $SrCoO_{2.5}$ has been controversial [12] due to the existence

Table 1. Cobalt–oxygen (Co–O) bond lengths as computed within the HSE and LSDA + U approaches, using different U parameters. O_{oct}, O_{tet} and O_{int} refer to the oxygen atoms in the octahedral, tetrahedral and intermediate layers, respectively, as labeled in figure 1.

	Co_{oct}–O_{oct} (Å)	Co_{tet}–O_{tet} (Å)	Co_{oct}–O_{int} (Å)	Co_{tet}–O_{int} (Å)
$U = 4$ (eV)	1.954	2.058	2.200	1.785
$U = 7.5$ (eV)	1.970	2.060	2.231	1.820
HSE	1.949	2.025	2.200	1.790

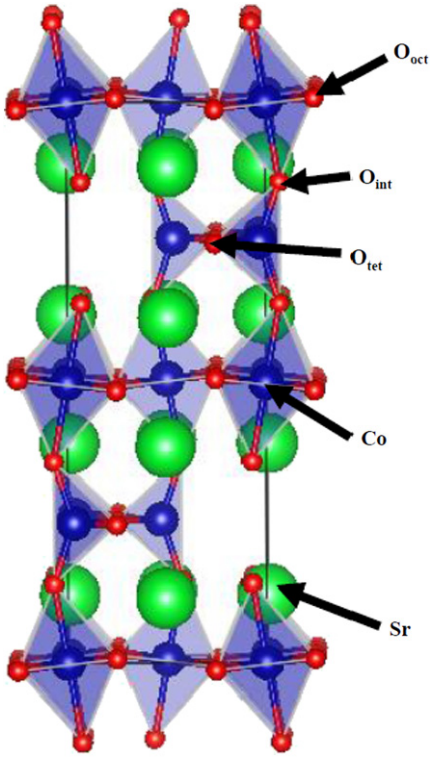

Figure 1. Crystal structure of $SrCoO_{2.5}$. The cobalt, oxygen and strontium atoms are represented by blue, red and green spheres, respectively.

of both the *Ima2* structure and the *Pnma* structure, we have used the *Ima2* structure in all our calculations, as this was predicted to be more stable by *ab initio* calculations [12]. We have used the experimental lattice constants: $a = 15.735$ Å, $b = 5.572$ Å, and $c = 5.466$ Å [12]. Although in a recent work [10] the c axis was chosen as the longer axis, this does not change the overall physics, and hence would not affect the results that are presented in this work. The presence of ordered oxygen vacancy 'channels' in $SrCoO_{2.5}$ modifies the crystal structure from its cubic perovskite phase. The Co–O bond length changes, which results in tilting of the Co–O polyhedra, as can be seen in figure 1. In table 1, we present the Co–O bond distances computed within the HSE and LSDA + U approaches, where two different values of U have been used.

The spin-polarized d states of Co_{oct} and Co_{tet}, and the O p states computed within the HSE approach are presented in figures 2(a), (b), and (c), respectively. We find an insulating ground state for $SrCoO_{2.5}$. The corresponding density of states plot for an LSDA + U calculation is presented in figure 3, where a U value of 7.5 eV has been used to match a band gap of about 0.6 eV within the HSE approach. Co in $SrCoO_{2.5}$ has a valency of +3 and therefore should have six valence electrons. However, as can be seen from figures 2(a)–(c), there is a strong mixing of the Co d and the O p states. Taking into account this hybridization, we find that Co effectively has seven electrons occupying its d states instead of six, hence validating the ligand–hole picture in this system. Furthermore, the fivefold d levels split due to the crystalline field, which no longer has a perfect octahedral or tetrahedral symmetry due to the Co–O polyhedral rotations, as shown in figure 1. The formation of a high-spin state on both Co_{oct} and Co_{tet} indicates that the exchange splitting dominates over the crystalline field splitting between the d levels.

3.1. Magnetic exchange parameters

We now move on to compute the magnetic exchange parameters. We assume that a Heisenberg Hamiltonian model describes the interaction between localized moments on the Co atoms as

$$H = -\sum_{ij} J_{ij}\mathbf{S_i}\cdot\mathbf{S_j} + E_0, \tag{3}$$

where the J are the interaction parameters, $\mathbf{S}$ indicates the localized spin on each site, and E_0 is an energy reference. The first-neighbor interaction between Co_{oct} atoms is referred to as J_1; the interaction among the Co_{tet} atoms is referred to as J_2; finally, the inter-planar interaction between Co_{oct} and Co_{tet} is J_3 (figure 3). Positive values for J indicate ferromagnetic interactions, and negative values mean antiferromagnetic interactions. We thus have four unknown parameters, J_1, J_2, J_3, and E_0, and hence would need four different configurations to determine them. The four different configurations that we used are shown in figures 4(a)–(d), where 4(a) represents the ferromagnetic (FM) configuration, and figures 4(b)–(d) represent the three different antiferromagnetic configurations, AFM (I), AFM(II), and AFM(III), respectively. The blue spheres represent the Co atoms that are octahedrally coordinated and the green spheres represent those that are tetrahedrally coordinated. The red spheres are the O atoms. Sr atoms have not been included in the picture.

Considering only nearest-neighbor interactions in the Hamiltonian (equation (3)), one can therefore write down four sets of equations which represent these four equations, as follows:

$$E_{FM} = E_0 - 4S^2J_1 - 2S^2J_2 - 2S^2J_3 \tag{4}$$

$$E_{AFM(I)} = E_0 - 4S^2J_1 - 2S^2J_2 + 2S^2J_3 \tag{5}$$

$$E_{AFM(II)} = E_0 - 4S^2J_1 + 2S^2J_2 \tag{6}$$

$$E_{AFM(III)} = E_0 + 4S^2J_1 - 2S^2J_2, \tag{7}$$

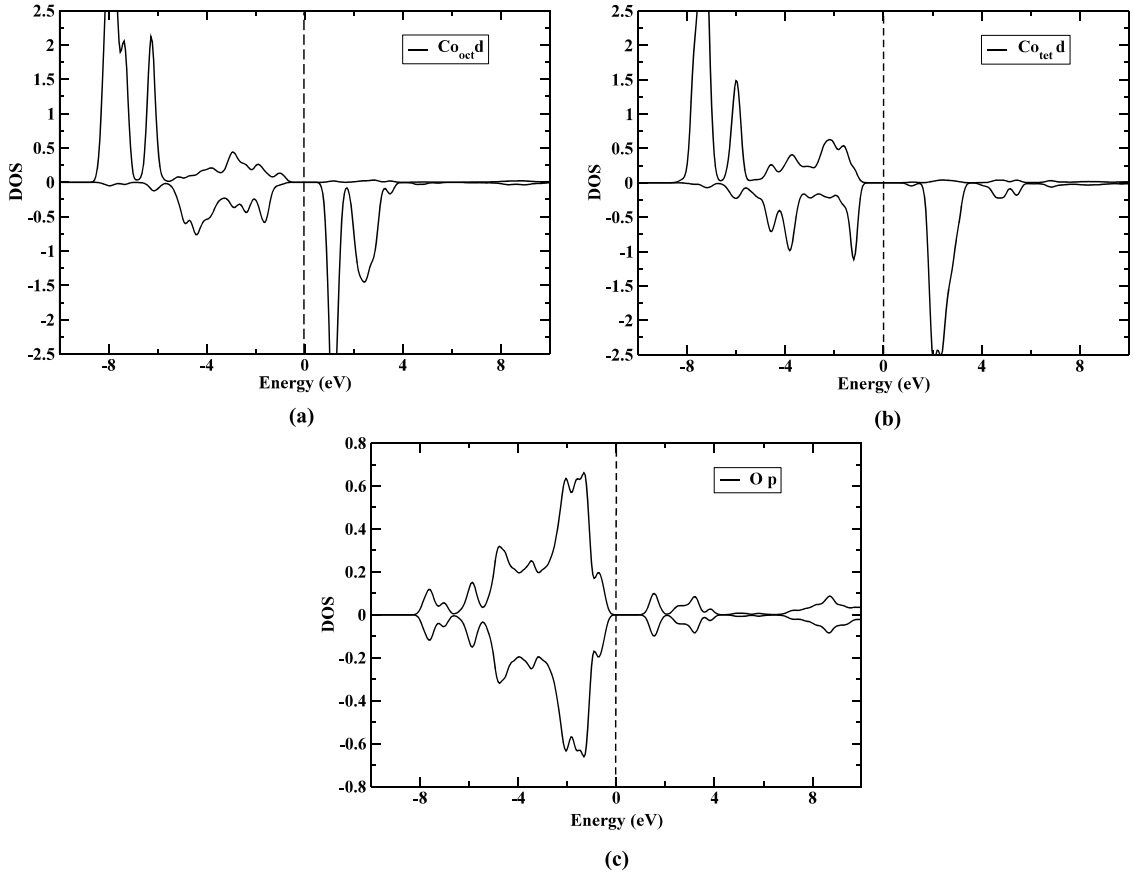

Figure 2. Partial density of states computed within the HSE approach. (a) d states of Co which are octahedrally coordinated (Co_{oct}). (b) d states of Co which are tetrahedrally coordinated (Co_{tet}). (c) O p states.

Table 2. Total energies of different magnetic configurations computed with HSE and LSDA + U functionals.

	HSE	$U = 7.5$	$U = 4$
E_{FM} (eV)	−352.22	−232.23	−242.52
$E_{AFM(I)}$ (eV)	−352.38	−232.43	−243.03
$E_{AFM(II)}$ (eV)	−352.50	−232.56	−243.32
$E_{AFM(III)}$ (eV)	−352.73	−232.78	−243.86

Table 3. The magnetic exchange interaction parameters.

	J_1 (meV)	J_2 (meV)	J_3 (meV)
$U = 4$ eV	−60	−61	−57
$U = 7.5$ eV	−25	−26	−22
HSE	−24	−22	−18

where $\mathbf{S} = 3/2$ for all of these equations. Equations (4) and (5) represent the configurations presented in figures 3(a) and (b), respectively. The other two configurations can be similarly set up. It must be pointed out that the Co atoms that are tetrahedrally coordinated are assumed to have two nearest neighbors (instead of four, as is the case for octahedral coordination) due to the absence of two O atoms. Upon solving equations (2)–(5) we obtain J_1, J_2, and J_3. We calculate the energies of each configuration with DFT. In tables 2 and 3 we present the total energies and the J values, computed within both LSDA + U and HSE approaches. As can be seen, the J values computed within the HSE approach match closely to a U value of 7.5 eV.

All the J values are found to be negative, implying antiferromagnetic interaction between the Co atoms. This confirms the super-exchange antiferromagnetic interaction between the Co d states mediated by the O p states and the experimental observation of $SrCoO_{2.5}$ being a G-type antiferromagnet. The G-type antiferromagnetic configuration is presented in figure 5 and is indeed found to have the lowest energy, in our calculations, when compared to all the other configurations presented above. We further checked the effect of supercell size on the magnetic interactions by employing a $1 \times 2 \times 2$ supercell and found that all our results converged to within 0.1 meV.

4. Spin waves

A detailed formalism for computing the spin-wave frequencies and intensities has been discussed elsewhere [15, 16, 26]. In this paper we will be using the same notation as used in [15]. Following the Holstein–Primakoff transformation, the spin operators S_{i+} and S_{i-} are transformed to boson creation and annihilation operators a_i and a_i^+ as $S_{i+} = \sqrt{2S}a_i$ and

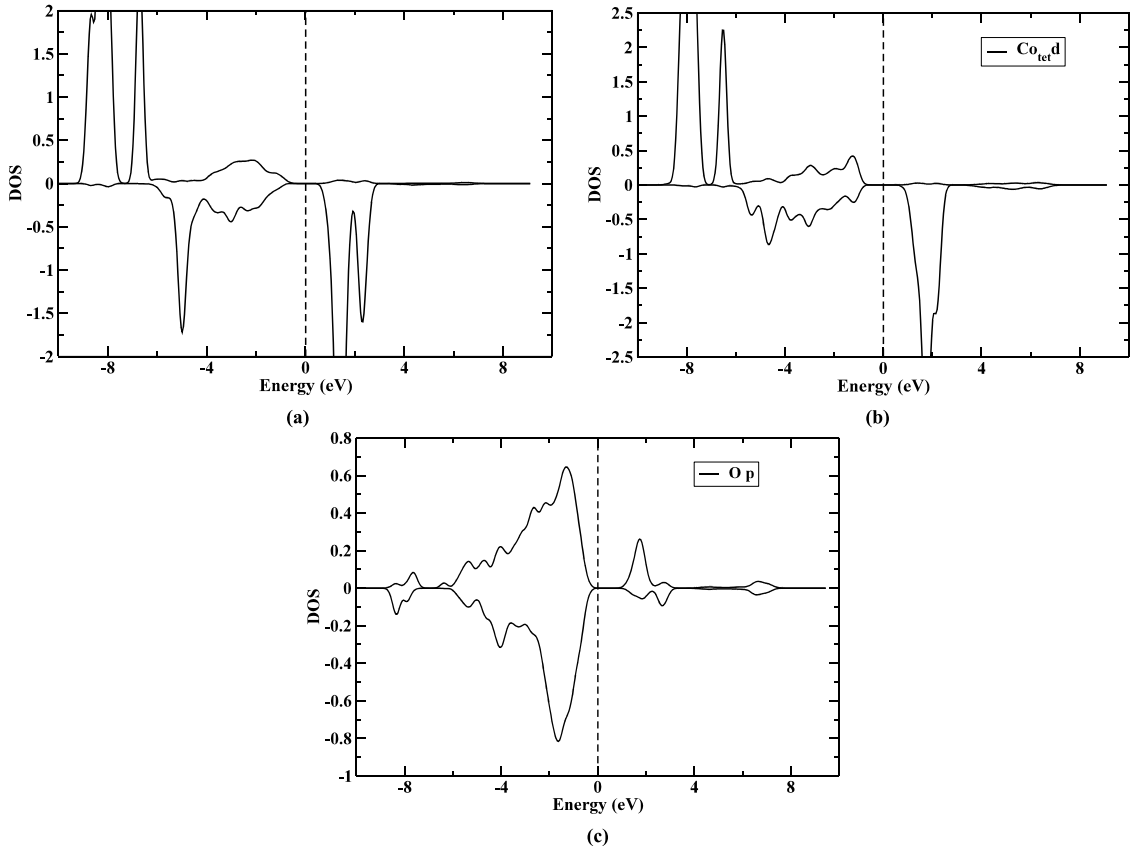

Figure 3. Partial density of states computed within the LSDA + U approach ($U = 7.5$ eV). (a) d states of Co which are octahedrally coordinated (Co_{oct}). (b) d states of Co which are tetrahedrally coordinated (Co_{tet}). (c) O p states.

$S_{i-} = \sqrt{2S}a_i^+$. Due to the spin structure of the G-type AF phase, the magnetic unit cell contains eight sublattices. The Hamiltonian H is expanded in powers of $1/\sqrt{S}$ about the classical limit as $H = E_0 + H_1 + H_2 + \ldots$. In this expansion of the Hamiltonian, E_0 is the classical energy and H_2 describes the dynamics of the spin waves (SWs). In equilibrium, H_1 must vanish.

In order to determine the SW frequencies, $\omega^{(r)}(\mathbf{k})$, one needs to solve the following equation:

$$i\mathrm{d}\mathbf{v}_\mathbf{k}/\mathrm{d}t = -[H_2, \mathbf{v}_\mathbf{k}] = M(\mathbf{k})\mathbf{v}_\mathbf{k}, \tag{8}$$

where $\mathbf{v}_\mathbf{k} = [a_\mathbf{k}^{(1)}, \ldots, a_\mathbf{k}^{(8)}, a_{-\mathbf{k}}^{(1)\dagger}, \ldots, a_{-\mathbf{k}}^{(8)\dagger}]$, and $M(\mathbf{k})$ is written as a $2s_t \times 2s_t$ matrix, $s_t = 8$ being the number of spin sublattices on four inequivalent layers. The SW frequencies, $\omega^{(r)}(\mathbf{k})$, are obtained from $\mathrm{Det}[M(\mathbf{k})N - \omega^{(r)}(\mathbf{k})I/2] = 0$, where N is a diagonal matrix with upper eight matrix elements $+1$ and lower eight matrix elements -1, and I is the 16-dimensional unit matrix. The dispersion relations for $\omega^{(r)}(\mathbf{k})$ are plotted in figure 6(a). Each of the four magnon modes is doubly degenerate.

Due to the missing Co–O bonds along the [110] direction, the solid branch of acoustic modes is higher between wavevectors (0, 0, 4) and (1, 0, 4) than between (0, 0, 4) and (0, 1, 4). While the solid branch vanishes at (0, 0, 4), (1, 0, 4), and (0, 1, 4), the dashed branch vanishes at (0, 0, 2).

We further determine the weight of each SW frequency from the eigenvectors of the matrix $M(\mathbf{k})$. The spin–spin correlation function $S(\mathbf{k}, \omega)$ can be expressed as a sum over delta functions at each SW frequency [15], and the inelastic neutron scattering intensity is given by

$$\begin{aligned} S(\mathbf{k}, \omega) &= \sum_{\alpha\beta} \left(\delta_{\alpha\beta} - \frac{k_\alpha k_\beta}{k^2}\right) S_{\alpha\beta}(\mathbf{k}, \omega) \\ &= \sum_r \delta(\omega - \omega^{(r)}(\mathbf{k}))A_r(\mathbf{k}). \end{aligned} \tag{9}$$

The second term implies that the observed spin excitations are polarized transverse to the momentum $\mathbf{k}$.

For the solid branch of acoustic modes, the SW intensity $A_r(\mathbf{k})$ plotted in figure 6(b) diverges at the ordering wavevectors (1, 0, 4) and (0, 1, 4). This acoustic mode vanishes at (0, 0, 4). On the other hand the dashed acoustic mode always has zero weight. Whereas the dash–dotted optical mode with frequency between 45 and 52 meV dominates the SW spectrum near (0, 0, 4), the short-dashed optical mode become visible slightly away from (0, 0, 4), including (1/2, 1/2, 4).

5. Conclusions

In conclusion, we have performed a first-principles study of the electronic structure and magnetic properties of $SrCoO_{2.5}$, employing hybrid functional and LSDA + U approaches. We find Co to be in high-spin state. The ground-state magnetic

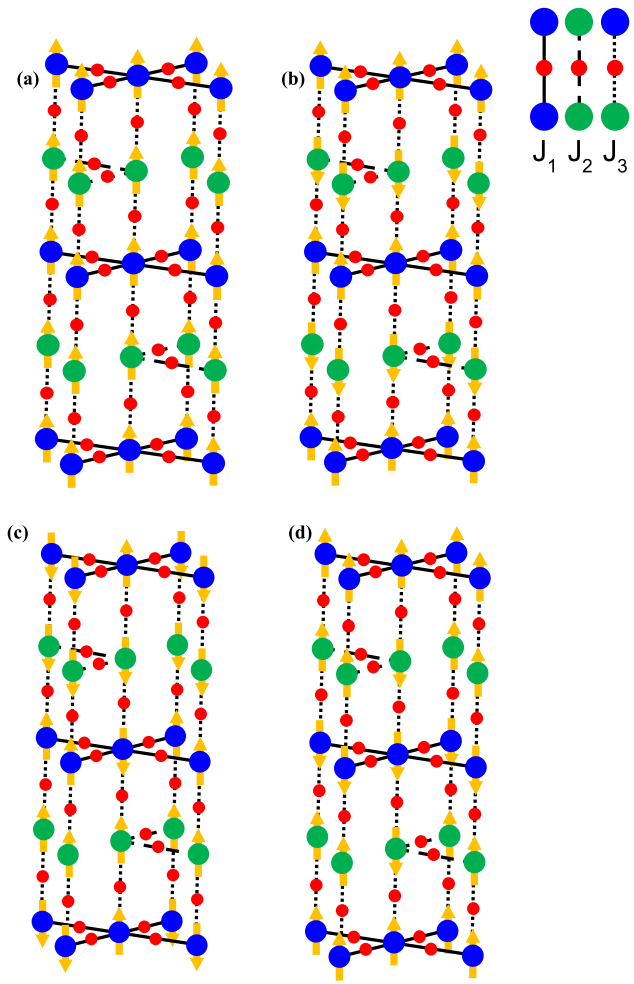

Figure 4. Different magnetic configurations used in calculating the exchange parameters J_1, J_2 and J_3. The spin directions are indicated by the arrows. (a) FM. (b) AFM(I). (c) AFM(II). (d) AFM(III).

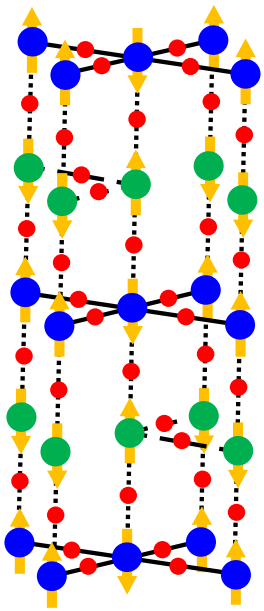

Figure 5. G-type antiferromagnetic structure.

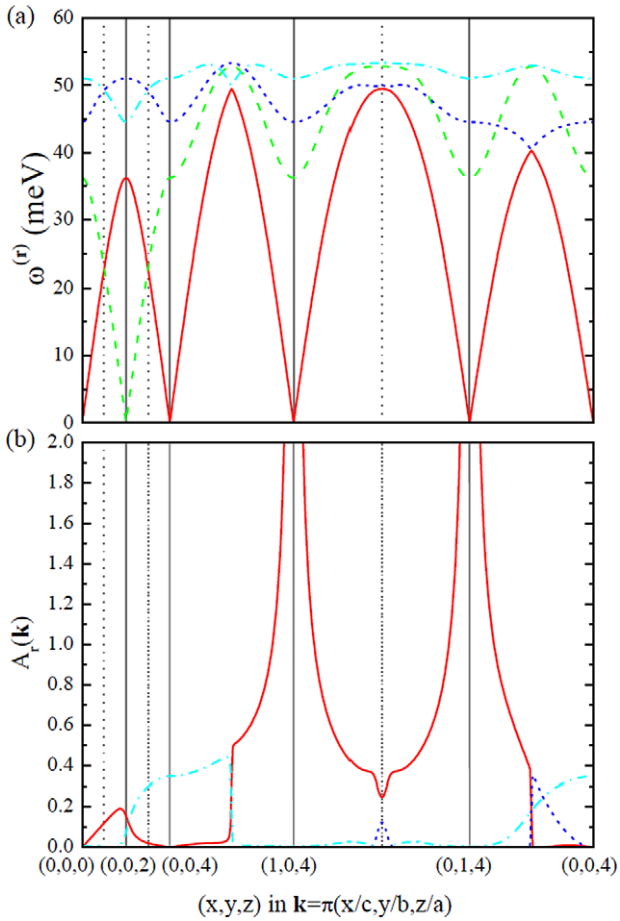

Figure 6. (a) Predicted spin-wave frequencies $\omega^{(r)}$. (b) Corresponding inelastic neutron scattering intensities, $A_r(\mathbf{k})$, as a function of momentum. Parameters used are the J_1, J_2 and J_3 computed within the HSE approach, as presented in table 3.

exchange interaction parameters were computed and the Holstein–Primakoff expansion was employed to predict the SW dispersion as well as the structure factor of this system. Our study confirms the G-type magnetic configuration where all the parameters are found to be negative.

The structure and magnetic properties of brownmillerite compounds and the effects of doping them with different magnetic elements have been a subject of great interest, for example in the case of $Ca_2Fe_{1-x}Mn_xAlO_{5+\delta}$. In future works it would be interesting to study the effect on the valence and spin state of Co while doping this material with electrons or holes. This in turn would affect the magnetic exchange between the Co atoms. A detailed understanding of this could enable us to 'design' different magnetic states within this oxygen-deficient cobaltite and further make this a potential material for important device applications.

Acknowledgment

This work was supported by the US Department of Energy, Basic Energy Sciences, Materials Sciences and Engineering Division.

References

[1] Lines M E and Glass A M 1977 *Principles and Applications of Ferroelectrics and Related Materials* (Oxford: Clarendon)

[2] Johnsson M and Lemmens P 2006 Crystallography and chemistry of perovskites *Handbook of Magnetism and Advanced Magnetic Media* ed H Kronmüller (New York: Wiley) (arXiv:cond-mat/0506606)

[3] Koonce C S, Cohen M L, Schooley J F, Hosler W R and Pfeiffer E R 1967 *Phys. Rev.* **163** 380

[4] Witze A 2010 Building a cheaper catalyst *Science News* Web Edition

[5] Shao Z P and Haile S M 2004 *Nature* **431** 170

[6] Cava R J, Takagi H, Krawjewski J J, Peck W F Jr and Hwang H Y 1993 *Phys. Rev.* B **47** 11525

[7] Stolen S, Bakken E and Mohn C E 2006 *Phys. Chem. Chem. Phys.* **8** 429

[8] Jeen H, Choi W S, Freeland J W, Ohta H, Jung C U and Lee H N 2013 *Adv. Mater.* **25** 3651–6

[9] Toquin R L, Paulus W, Cousson A, Prestipino C and Lamberti C 2006 *J. Am. Chem. Soc.* **128** 13161

[10] Jeen H *et al* 2013 *Nature Mater.* **12** 1057–63

[11] Takeda T and Watanabe H 1972 *J. Phys. Soc. Japan* **33** 973

[12] Muñoz A, de la Calle C, Alonso J A, Botta P M, Pardo V, Baldomir D and Rivas J 2008 *Phys. Rev.* B **78** 054404

[13] Long Y, Kaneko Y, Ishiwata S, Taguchi Y and Tokura Y 2011 *J. Phys.: Condens. Matter* **23** 245601

[14] Takeda T, Yamaguchi Y and Watanabe H 1972 *J. Phys. Soc. Japan* **33** 970

[15] Fishman R S, Haraldsen J T, Furukawa N and Miyahara S 2013 *Phys. Rev.* B **87** 134416

[16] Haraldsen J T and Fishman R S 2010 *J. Phys.: Condens. Matter* **22** 509801

[17] Kresse G and Furthmüller J 1996 *Phys. Rev.* B **54** 11169

[18] Blöchl P E 1994 *Phys. Rev.* B **50** 17953

[19] Monkhorst H J and Pack J D 1976 *Phys. Rev.* B **13** 5188

[20] Dudarev S L, Botton G A, Savrasov S Y, Humphreys C J and Sutton A P 1998 *Phys. Rev.* B **57** 1505

[21] Heyd J, Scuseria G E and Ernzerhof M 2003 *J. Chem. Phys.* **118** 8207
Heyd J, Scuseria G E and Ernzerhof M 2006 *J. Chem. Phys.* **124** 219906(E)

[22] Perdew J P, Burke K and Ernzerhof M 1996 *Phys. Rev. Lett.* **77** 3865

[23] Adamo C and Barone V 1999 *J. Chem. Phys.* **110** 6158

[24] Perdew J P, Ernzerhof M and Burke K 1996 *J. Chem. Phys.* **105** 9982

[25] Choi W S, Jeen H, Lee J H, Seo S S A, Cooper V R, Rabe K M and Lee H N 2013 *Phys. Rev. Lett.* **111** 097401

[26] Kubo R 1952 *Phys. Rev.* **87** 568